Asian Journal of Chemistry; Vol. 30, No. 11 (2018), 2437-2444

ASIAN JOURNAL OF CHEMISTRY

https://doi.org/10.14233/ajchem.2018.21434

Molecular Modeling of 4′,5-Disubstituted Biphenyl Acetic Acid Molecules for their Anti-inflammatory Activity through 3D-QSAR, Docking and Molecular Dynamics Simulation

ANANDA SARKAR[1] and ATISH DIPANKAR JANA[2,*]

[1]Department of Physics, Acharya Prafulla Chandra College, Kolkata-700 131, India
[2]Department of Physics, Behala College, Parnasree, Kolakata-700 060, India

*Corresponding author: E-mail: atish@behalacollege.in; atishdipankarjana@yahoo.in

Received: 8 May 2018; *Accepted*: 11 June 2018; *Published online*: 27 September 2018; AJC-19091

A set of 4′,5-di-substituted 3-biphenyl acetic acid (BPA) and α-methyl derivatives (MBPA) are powerful nonsteroidal anti-inflammatory and analgesic agents. 3D-QSAR analysis through CoMFA and CoMSIA procedures has been carried out for the chosen set of molecules. The CoMSIA analysis reveals that the steric field is more important than the electrostatic field whereas the CoMSIA analysis reveal the importance of hydrophobic field. The docking analysis reveals that besides the hydrogen bonding interaction, π···π and CH···π interactions are also responsible for binding of the molecules in the binding pocket of the COX2 protein (1CX2.pdb). Molecular dynamics (MD) simulation has been performed for the most efficiently bound molecule in the cavity of the COX2 protein. The most stable conformation of the molecule found in molecular dynamics study matches well with its conformation and binding mode obtained from the docking study.

Keywords: COX-inhibition, 3D-QSAR, Molecular docking, Molecular dynamics.

INTRODUCTION

Cyclooxygenase, commonly known as COX, converts arachidonic acid to prostaglandin. Arachidonic acid is formed in the process of lipid metabolism through the catalytic activity of lypooxygenase. COX, first converts arachidonic acid to prostaglandin-H_2 (PGH_2) and then to various other prostanoids like PGE_2, PGD_2, $PGF_{2\alpha}$, PGI_2 as well as thromboxane TXA_2 [1]. Prostaglandins are the effective mediators of inflammation and also produce hypersensitive life-threatening allergic reactions [2]. COX occurs in two different isoforms, namely COX-1 and COX-2. COX-2 has nearly 60 % homology with COX-1 in gene sequence. COX-1 is always present in most cells and performs protective housekeeping role in the production of prostanoids. One of the important functions of COX-1 is to protect and maintain gastrointestinal tract. COX-2 is generally induced by inflammatory stimuli and is responsible for nearly 20 times elevated production of prostaglandins [3]. The elevated production of prostaglandin is responsible for redness, heat, swelling and pain, all associated with inflammation. Nonsteroidal anti-inflammatory drugs (NSAID) efficiently inhibit COX-2 and are commonly used during fever and pain. These are also notorious for their side-effects as during inhibition of COX-2 by NSAID, COX-1 is also inhibited undesirably, causing gastrointestinal problems. Thus, search is on for finding selective inhibitors of COX-2 that can act as potential NSAID drug molecules [4]. Many set of molecules have been explored for this purpose having core scaffold based on indole [5-8], pyrrole [9], triazole [10], pyridine [11,12], coumarin [13], pyrazolin [14], quinoline [15], oxadiazole [16], thiadiazole [17], thiophenecarboxamide [18] as well as natural compounds like flavonoids [19].

Recently, we have reported the two dimensional quantitative structure activity relationship (2D-QSAR) model for the anti-inflammatory activities of a set of 4′,5-di-substituted 3-biphenyl acetic acids (BPA) and several α-methyl derivatives (MBPA) of it. In this QSAR model, nucleus independent chemical shift (NICS) was used as a novel molecular descriptor and was introduced for the first time [20] in a 2D-QSAR model. Two other descriptors used in this model are relative Fuki function and frontier electron density. The obtained model nicely predicted the activity of the chosen set of molecules and had a good predictive capacity. A successful 2D-QSAR model employing NICS indicated that the aromatic rings present in the molecules

should somehow be involved in the intermolecular interactions. To gain more insight into the 3D interacting nature of the BPA and MBPA molecules in their COX-2 inhibition activities, in the present work we have attempted to construct 3D-QSAR models along with molecular docking and molecular dynamics studies.

In 3D-QSAR, comparative molecular field analysis (CoMFA) [21] and comparative molecular similarity indices analysis (CoMSIA) have been carried out [22,23] to predict the inhibitory activities of the compounds. This study has also provided information regarding the important regions over the molecular surface where interactive fields are responsible for the activities of molecules.

Docking studies provide valuable information regarding the nature of intermolecular interactions of a drug molecule in the active site of suitable protein [24-26] for a specific pharmacological activity. Docking studies have been performed for all the molecules under consideration which were docked into the binding site of the COX-2 protein (1CX2.pdb) using Surflex-Dock module of Sybyl-X software package [27]. This has provided a clear view of the interactions between the COX-2 protein and the inhibitor molecule. Docking studies are often supplemented by molecular dynamics study which provides information regarding the dynamical nature and time scale of stabilization of the drug molecule in the binding cavity of the protein molecule [28,29]. A molecular dynamics (MD) study has been performed here, in which the most active molecule has been excited and subsequently allowed to relax in the same binding pocket of the COX-2 protein. The molecule reaches the equilibrium conformation within 4 nano second and the final conformation nicely matches with that found in the docking analysis.

The QSAR model, docking analysis and molecular dynamics study have provided molecular level insight into the structure-activity relationship of the BPA class of molecules as potential COX-2 inhibiting agents.

EXPERIMENTAL

Selection of dataset: A series of 4′,5-disubstituted 3-biphenylacetic acids (BPA) and several α-methyl derivatives (MBPA) of it, whose anti-inflammatory activity (CPE %) have been measured through experiments on SLC-SD rats using carrageenan-induced rat paw edema has been taken from the literature [30] and listed in Table-1. CPE % values of the molecules were transformed into log (CPE %), which ranged from 0.60 to 1.72. A test set of four molecules have been used to determine the external predictivity of the resulting QSAR model and these were removed from the original data set. The chosen test set evenly spanned the anti-inflammatory activity range as well as the chemical structural diversity of the database.

3D-QSAR (CoMFA and CoMSIA) analysis

Alignment of molecules: Alignment of the relevant set of molecules is an important part of the development of successful CoMFA and CoMSIA models [31]. In the present study ligand based alignment technique has been chosen in which a template molecule is first isolated over which remaining molecules are aligned. Here molecule no 19 which shows the highest activity within the dataset has been used as the template. The aligned set of molecules is depicted in Fig. 1.

CoMFA and CoMSIA setup: Utilizing the aligned set of data both CoMFA and CoMSIA models have been built separately. To generate the CoMFA and CoMSIA molecular descriptor fields a 3D cubic lattice has been employed. Grid spacing of the lattice was set at 1 Å and the lattice extended 4 Å beyond the aligned set of molecules in every direction. Tripos force field was utilized to calculate the van dar Waals potential as well as the Coulombic terms. A sp^3 hybridized carbon atom

TABLE-1
MOLECULAR STRUCTURE OF BPAs AND MBPAs AND THEIR ANTI-INFLAMMATORY ACTIVITIES

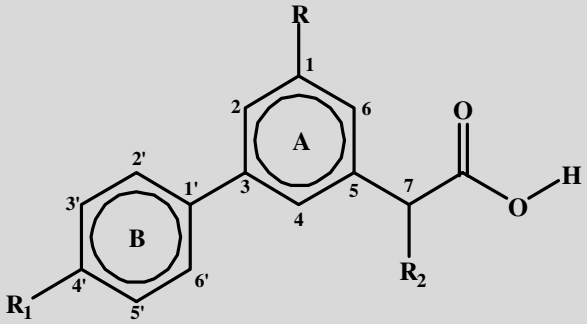

S. No.	R	R_1	R_2	log (CPE %)	S. No.	R	R_1	R_2	log (CPE %)
1	NHOAc	H	H	0.70	11	F	Cl	H	1.58
2#	NHOAc	MeO	H	1.18	12	H	H	Me	1.23
3	NH_2	Cl	H	1.20	13#	H	Cl	Me	1.54
4	H	H	H	1.67	14#	Cl	H	Me	0.60
5	H	MeO	H	1.04	15	Cl	MeO	Me	0.90
6	H	Cl	H	1.64	16	Cl	Cl	Me	1.61
7	Cl	H	H	1.51	17	F	H	Me	1.49
8	Cl	MeO	H	1.28	18#	F	Cl	Me	1.59
9	Cl	Cl	H	1.65	19	Me	Cl	H	1.72
10	F	H	H	1.70	–	–	–	–	–

#test set of molecules

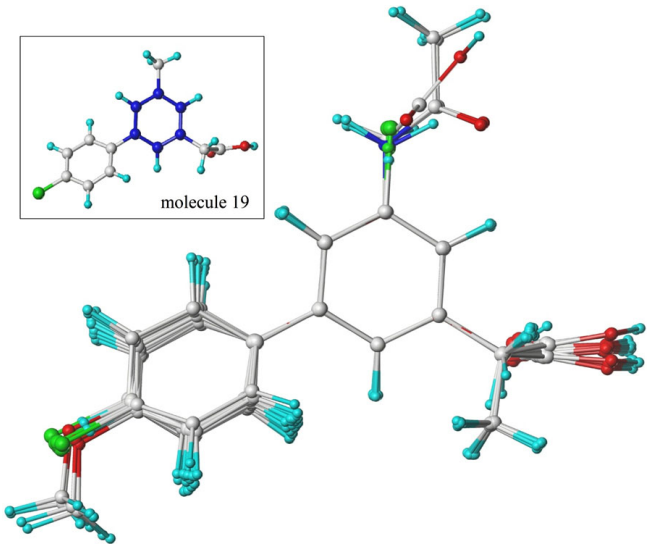

Fig. 1. Molecules have been aligned over the template molecule 19 which is shown in the inset. The common moiety is one of the the phenyl groups marked blue

with a charge of +1 was taken as the probe atom for calculating the steric and the electrostatic fields in the CoMFA model. Truncation limit for energy values were set at 30 kcal/mol. In the CoMSIA method we have used the same lattice box. A probe atom having radius 1.0 Å with charge +1 was utilized for integration of steric, hydrophobic, electrostatic, hydrogen bond donor and hydrogen bond acceptor fields. Both hydrophobic as well as hydrogen bond properties were set at +1. Attenuation factor was taken to be its default value which is 0.3.

Derivation and validation of the model: Partial least squares (PLS) was used to find the linear relationship between the CoMFA fields and the pIC_{50} values. Another linear relationship was established between CoMSIA fields and pIC_{50} values in a similar manner. Leave-one-out (LOO) method was the basis of cross-validation analysis. The general procedure adopted here is to remove one molecule from the data set and predict its activity from a model based on the rest of the data set [32]. For determining optimum number of components (ONC), PLS was combined with the cross-validation option. ONC were then used in deriving the final CoMFA and CoMSIA models without cross-validation. ONC is the number of components resulting in highest cross-validated correlation coefficient (r_{cv}^2 or q^2). In the cross-validation procedure a default value of 2.0 kcal/mol was set for column filtering. Non-cross-validated analysis with the ONC was used to derive the final models along with its correlation coefficient r^2. A test set of seven molecules not included in the training set was employed to test the predictive ability of the model thus found. For predicting the pIC_{50} values, these seven molecules were aligned to the template molecule. Equation 1 was employed to compute the predictive correlation coefficient (r^2_{pred}), based on the molecules of the test set.

$$r^2_{pred} = 1 - \frac{\sum (Y_{obs(test)} - Y_{pred(test)})^2}{\sum (Y_{obs(test)} - \bar{Y}_{training})^2} \quad (1)$$

where $Y_{pred(test)}$ and $Y_{obs(test)}$ are the predicted and observed activity values of the test set molecules. $\bar{Y}_{training}$ indicates the mean activity value of the training set molecules. The value of r^2_{pred} for an acceptable model should be greater than 0.5 [33].

Molecular docking: Molecular docking studies offer useful insight into the nature of interaction between the ligand and the relevant protein residue. Docking study most often come as a very useful guide in the drug design process. To investigate the protein-ligand interactions, all the molecules, both training and tests were docked in the binding site of cyclooxygenase-2 (COX-2) using Surflex-Dock module of Tripos Inc. [27]. Crystal structure of COX-2 (1CX2) was obtained from the Protein Data Bank. The protein structure was utilized in the docking experiment without energy minimization. All ligands and water molecules of the receptor protein were removed and the polar hydrogen atoms were added. The establishment of protomol has been performed using the 'automatic' option in the Sybyl-X package which finds the largest cavity in the receptor protein. To visualize the binding mode between the protein and ligand, the Molecular Computer Aided Design (MOLCAD) program, implemented in SYBYL-X [27], was employed.

Molecular dynamics (MD) simulation: Molecular dynamics simulation study has been carried out with the help of Sybyl X software package. Compound **2** which has the highest Surflex-X score in docking study was chosen for the MD simulation. AMBER7 FF99 force field was used for energy minimization in this procedure. Gasteiger-Hückel charges was used for the chosen molecule. Initial velocity distribution was taken to be a Boltzmann type distribution. Molecular dynamics simulation was performed for 20 ns with a time step of 10 fs. Snapshot of the conformation at every 2 ps were utilized to calculate RMSD values.

RESULTS AND DISCUSSION

3D-QSAR studies: The statistical parameters for the CoMFA model have been listed in Table-2. The CoMFA model using both steric and electrostatic fields has a cross-validated correlation coefficient (q^2) of 0.485 with an optimized component of six. The obtained model has a high non-cross-validated correlation coefficient (r^2) of 0.909 and quite a low standard error estimate (SEE) of 0.144. The model also has a good F value of 19.133. The contributions of steric and electrostatic fields were 0.364 and 0.636, respectively. The actual and predicted log (CPE %) values of the training set and the test set by the derived CoMFA model have been presented in Table-3. The graph of actual activity *versus* predicted log (CPE %) of the training set and the test set is illustrated in Fig. 2.

TABLE-2
PLS RESULTS OF CoMFA AND CoMSIA MODELS

PLS statistics	CoMFA	CoMSIA
q^2	0.485	0.770
r^2	0.909	0.861
r^2_{pred}	0.547	0.610
ONC	06	4
SEE	0.144	0.141
F value	19.133	15.426
Field contribution		
Steric	0.364	0.549
Electrostatic	0.636	–
Hydrophobic	–	0.451

TABLE-3
PREDICTED ACTIVITY VALUES FROM THE CoMFA, CoMSIA MODELS AND THE DOCKING SCORES

S. No.	Obsd Acit	CoMFA		CoMSIA		S. No.	Obsd Acit	CoMFA		CoMSIA	
		Pred Act	Res	Pred Act	Res			Pred Act	Res	Pred Act	Res
01	0.70	0.97	-0.27	0.88	-0.18	11	1.58	1.59	-0.01	1.60	-0.02
02#	1.18	1.33	-0.15	1.23	-0.05	12	1.23	1.09	0.14	1.26	-0.03
03	1.20	1.52	-0.32	1.62	-0.42	13#	1.54	1.38	0.16	1.31	0.23
04	1.67	1.67	0.00	1.66	0.01	14#	0.60	1.06	-0.46	0.99	-0.39
05	1.04	1.39	-0.35	1.28	-0.24	15	0.90	1.00	-0.10	0.88	0.02
06	1.64	1.53	0.11	1.63	0.01	16	1.61	1.61	0.00	1.53	0.08
07	1.51	1.63	-0.12	1.54	-0.03	17	1.49	1.61	-0.12	1.53	-0.04
08	1.28	1.45	-0.17	1.28	0.00	18#	1.59	1.60	-0.01	1.51	0.08
09	1.65	1.44	0.21	1.61	0.04	19	1.72	1.44	0.28	1.64	0.08
10	1.70	1.67	0.03	1.69	0.01	–	–	–	–	–	–

#test set of molecules

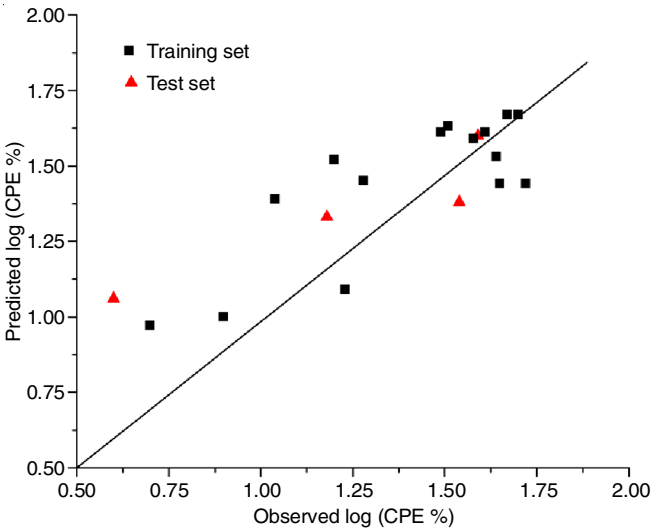

Fig. 2. Graph of observed and predicted activity values from the CoMFA model

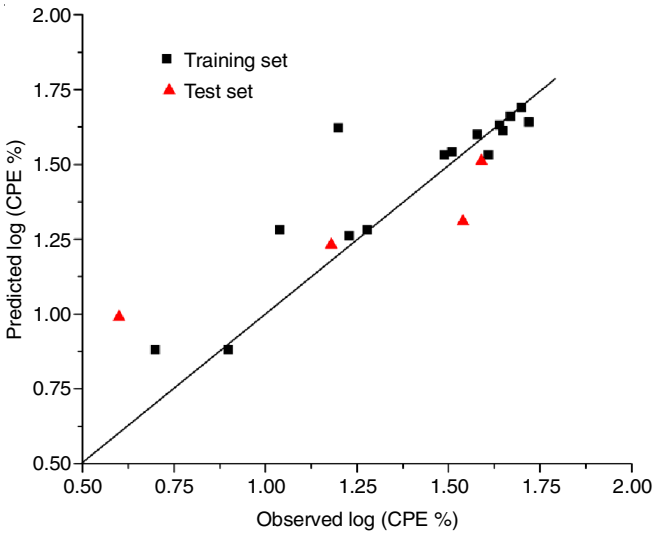

Fig. 3. Graph of observed and predicted activity values from CoMSIA model

In CoMSIA model, five CoMSIA descriptors in different combinations change the model significance and predictivity. For this reason, all 31 possible descriptors' combinations were calculated with associated parameters. The best CoMSIA model is based on steric and hydrogen bond acceptor fields and has the highest q^2 value (0.770) and a high non-cross-validated correlation coefficient r^2 of 0.861 with a low SEE value of 0.141 and F value of 15.462. Contributions of steric and hydrophobic fields were 0.549 and 0.451, respectively. All the statistical parameters for the CoMSIA model have been listed in Table-2. The actual and predicted log (CPE %) values of the training set and the test set by the CoMSIA model is given in Table-3 and the graph of actual activity *versus* predicted log (CPE %) of the training set and the test set has been illustrated in Fig. 3.

The calculated results of external validation for CoMFA and CoMSIA models are listed in Table-2. It is revealed by this external validation that both the model exhibit high predictive power and are reliable for predicting the activity of a new molecule.

Interpretation of the 3D-QSAR models: The CoMFA steric and electrostatic contour maps are shown in Figs. 4 and 5, respectively. These maps specify the regions in 3D space around the molecules where changes in the steric and electrostatic fields would increase or decrease the activity. The steric

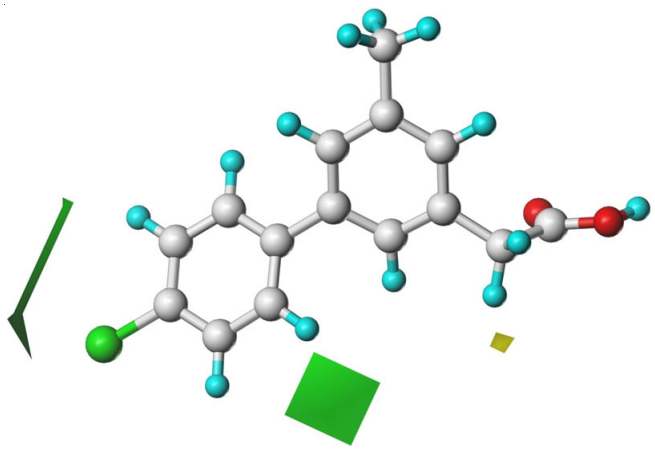

Fig. 4. CoMFA steric contour map for the reference molecule 19

field is represented by green and yellow contours. Green contours indicate regions where bulky groups are favourable for increased activity and the yellow contours represent regions where less bulky groups are desirable for better activity. From Fig. 4 one can see that green contours are a bit away from the 4′-phenyl moiety but the yellow contour are closer to the R″ group. This indicates that less bulky substituent as R″ is necessary for increased activity. This correlates well with molecules

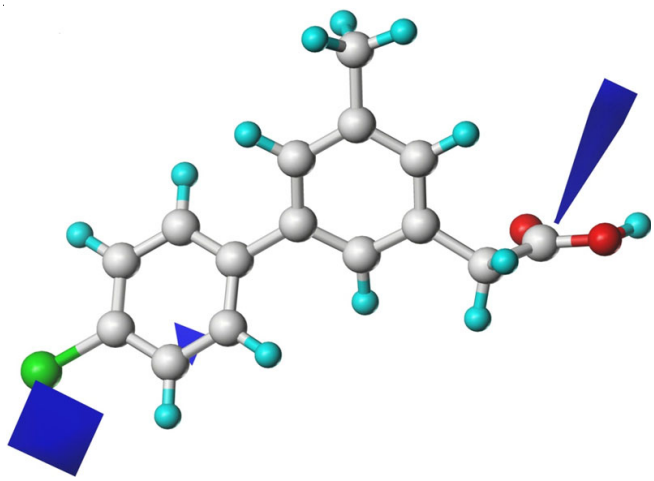

Fig. 5. CoMFA electrostatic contour map for the reference molecule 19

19, 10, 4, 9, 6 which belong to top five active molecules having R″ = H.

In the CoMFA electrostatic contour maps (Fig. 5) prominent blue contours appear surrounding the R′ group. This indicates that electropositive donor atoms on the receptor protein will suitably bind the electronegative substitutions at the position of R′ which will act as complementary acceptors. Molecules 6, 9, 11, 13, 16 and 19 all of which has R′ = Cl show comparatively higher activities and correlate well with the above observations.

The CoMSIA analysis reveals that the steric and hydrophobic fields constitute the best 3D-QSAR model with a contribution of 54.9 and 45.1 %, respectively. The CoMSIA steric map is depicted in Fig. 6, which shows prominent green contours right at the positions of R′ and R″. There is also a small green region close to the position of R. Green contours are the regions where a bulky substitution is preferred for better activity. Molecules 16 and 18 having R″ = CH_3 group show relatively higher activity.

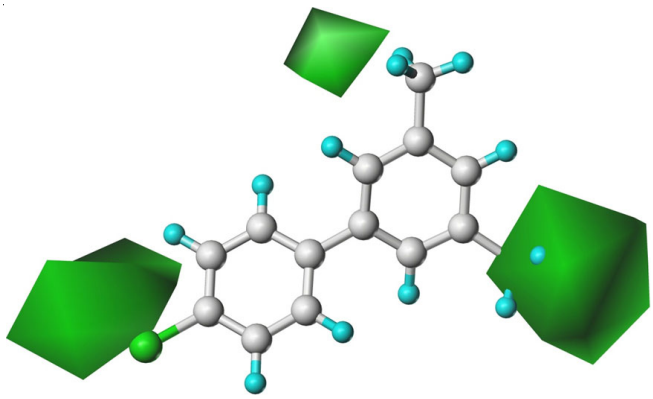

Fig. 6. CoMSIA steric field for the reference molecule 19

The CoMSIA hydrophobic field has been depicted in Fig. 7, which shows two prominent white contours at the positions of R′ and R″. White contours represent regions that would favour hydrophilic groups. Molecules 8, 9, 10, 16 and 18 which has either F or Cl as substitution at the position of R show comparatively higher activities as F or Cl can act as hydrophilic groups. Similarly molecules 4, 6, 9, 10 and 19 which has R″ = H also show higher activities.

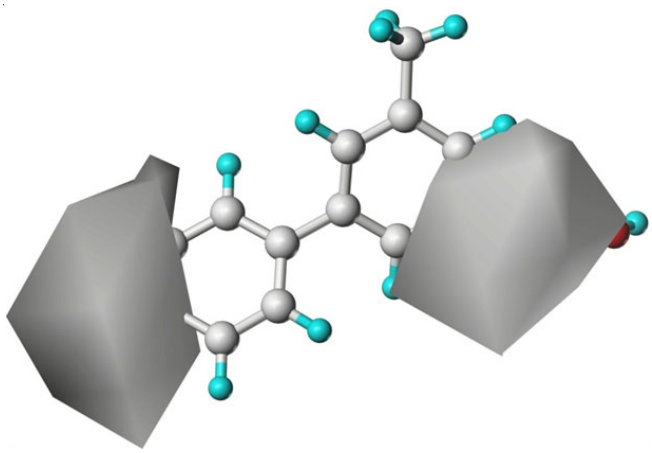

Fig. 7. CoMSIA hydrophobic field for the reference molecule 19

Docking analysis: All molecules comprising the training and the test sets were docked in the binding site of COX-2 protein (1CX2) using Surflex-Dock module of Tripos Inc. [27]. The results show that the molecule 2 has highest Surflex-score 8.29. Thus to remain brief we present here the binding mode of molecule 2 at the active site of the protein 1CX2. As shown in Fig. 8, the hydrogen bonding interaction and CH···π interaction is responsible for the binding of the molecule in the active site of the protein. There exist three hydrogen bond contacts (i) one between the carboxylate carbonyl attached to the A-ring of the ligand which act as acceptor for the amino (–NH_2) donor of arginin120 [the N···O distance is 2.902 Å; H···O distance is 2.009 Å and the NH···O angle is 147.46°] (ii) the second one between amino-acetate carbonyl and tyrosin385 where carbonyl O act as acceptor for tyrosin OH proton [the O···O distance is 2.858 Å; H···O distance is 2.038 Å and the NH···O angle is 142.22°] and (iii) the third one between methoxy oxygen and histidine90 where the imidazole NH proton is donated to methoxy O acceptor [the N···O distance is 2.806 Å; H···O distance is 1.881 Å and the NH···O angle is 155.10°]. Both the aromatic rings of the ligand are involved in CH···π interactions. One of the methyl hydrogen atoms attached to valine349 interact with the phenyl ring A of the ligand. The C···π_{cga} (π_{cga} is the centroid of ring A) distance is 3.642 Å H···π_{cga} distance

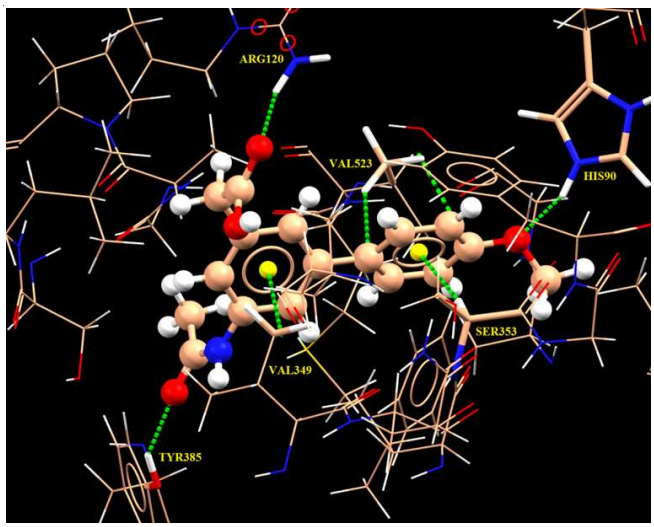

Fig. 8. Binding mode of molecule 2 at the active site of the protein 1CX2

is 2.741 Å and C-H···π_{cga} angle is 138.90°. The second aromatic ring of the ligand is involved in sandwiched C-H···π interaction where both faces of the ring B interact with protein residues. On one side the methyl hydrogen of the Valine523 come closer (C···π_{cgb} distance 3.681 Å; H···π_{cgb} distance is 3.037 Å and C-H···π_{cgb} angle is 117.82°) whereas on the other side –CH group of the Ser353 interacts with the ring C···π_{cgb} (π_{cgb} is the centroid of ring B) distance is 3.531; H···π_{cgb} distance is 2.463 Å and C-H···π_{cgb} angle is 163.46°.

Further, the MOLCAD surfaces of the binding site of 1CX2 have been developed to show the hydrogen bonding sites (HB) (Fig. 9a), electrostatic potential (EP) (Fig. 9b), lipophilic potential (LP) (Fig. 9c) and cavity depth (CD) (Fig. 9d). The molecular electrostatic potential on a protein surface can be used to find the areas that act as attraction sites for the regions of the ligand having matching opposite colours. The red colour shows the electron-withdrawing zone and purple colour shows electron-donating zone. The interactions depicted for hydrogen bonding contacts in Fig. 8 correlate to that of the CoMFA electrostatic contour map.

Molecular dynamics simulation: To further confirm the reliability of docking results, MD simulation has been performed to explore the probable binding modes of the ligand with the receptor protein. This investigation was performed for one of the highly active molecule 2 which has the highest Surflex X score in the docking study. Molecule 2 was first excited and subsequently allowed to relax in the binding site of the cyclooxygenase (PDB ID: 1CX2) with an aim to find out the most stable conformation of molecule 2 in the binding site. A 20 ns simulation of the ligand-receptor complex was found to

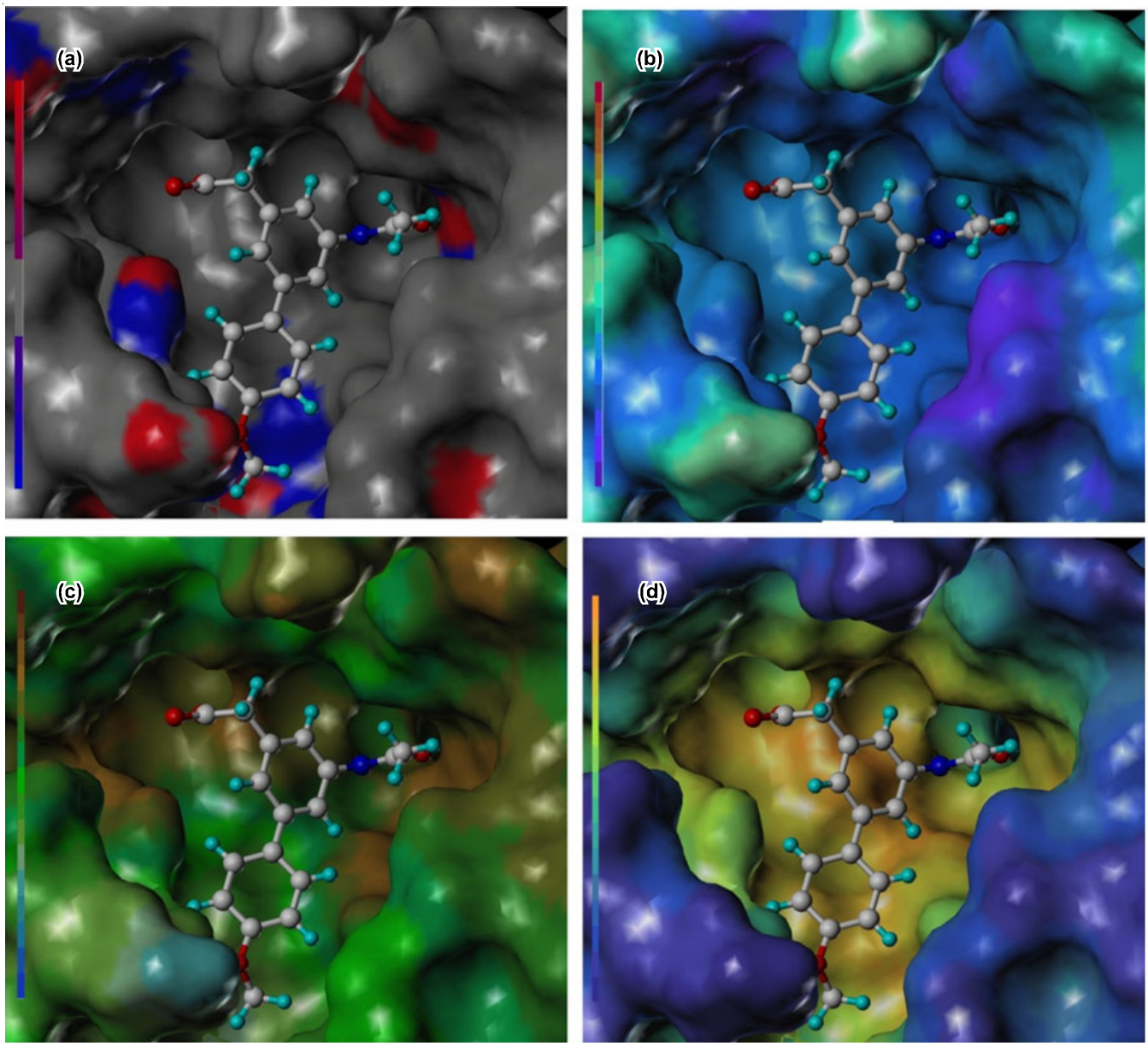

Fig. 9. MOLCAD surfaces of the binding site of 1CX2 with molecule 2. (a) Hydrogen bonding sites surface (HB); c) colour ramp ranges from red (hydrogen bond donors) to blue (hydrogen bond acceptors) (b Lipophilic potential (LP); colour ramp ranges from brown (highest lipophilic surfacse) to blue (highest hydrophobic surfaces) (c) Electrostatic potential (EP); colour ramp ranges from red (most positive) to purple (most negative) (d) Cavity depth (CD); colour ramp ranges from blue (low depth values, outside the pocket) to light red (high depth values deep, cavities deep inside the pocket)

be sufficient to extract the necessary information. The root mean square deviation (RMSD) characterizing the quality of the simulation has been depicted (Fig. 10). After 4 ns, the RMSD of the complex reaches about 6 Å and fluctuates around this with a deviation of about 2 Å. This indicates that the docked complex can reach metastable conformation within around 4 ns of simulation. The MD-simulated equilibrium structure of molecule 2 and the original docked pose of the same has been shown in Fig. 11. Alignment of the simulated ligand (red) on the docked pose of it (green) shows that there is only a slight difference between these two conformations. The number of hydrogen bonds that the molecule forms with the protein backbone remains three.

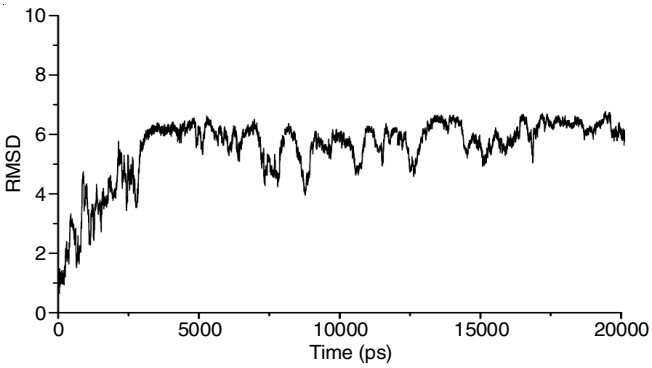

Fig. 10. Root-mean-square deviation (RMSD) of the docked ligand complexed with 1CX2 *versus* the MD simulation time

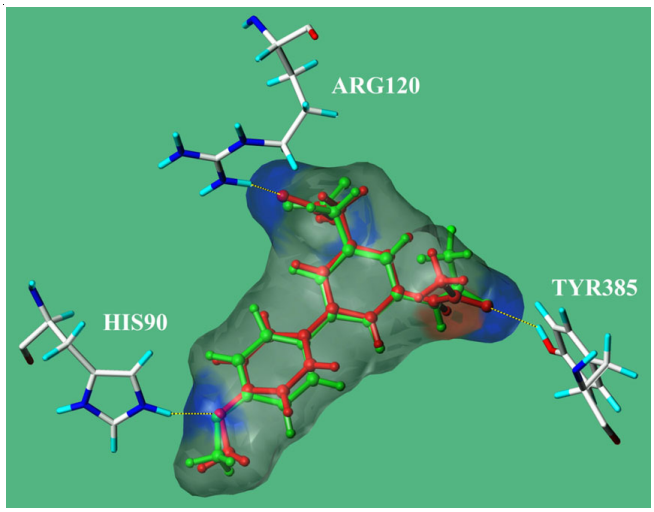

Fig. 11. Alignment of simulated ligand (red) on unsimulated ligand (green) complexed with 1CX2 protein

These three hydrogen bond contacts are (i) between the carboxylate carbonyl attached to the A-ring of the ligand which act as acceptor for the amino ($-NH_2$) donor of arginin120 [the N···O distance is 3.262 Å; H···O distance is 2.380 Å and the NH···O angle is 1446.73°] (ii) the second one between amino-acetate carbonyl and tyrosin385 where carbonyl O act as acceptor for tyrosin OH proton [the O···O distance is 2.908 Å; H···O distance is 2.082 Å and the NH···O angle is 143.28°] (iii) and the third one between methoxy oxygen and histidine90 where the imidazole NH proton donated to methoxy O acceptor [the N···O distance is 2.728 Å; H···O distance is 1.790 Å and the NH···O angle is 163.17°].

The MD analysis described above suggests that there are no significant differences between the original docked structure and the MD-simulated structure. Therefore, the docking study and the molecular dynamics study well complement each other.

Conclusion

In continuation of our previous study of the anti-inflammatory activity of a set of BPA and MBPA molecules using a 2D-QSAR model with NICS as a successful molecular descriptor we have augmented the model to a 3D one. Both CoMFA and CoMSIA models have been derived. CoMFA analysis shows that the setric effect is more dominant than the electrostatic effect. Less bulky substituents at R is preferred over bulky substitution for better activity. Similarly more electron rich substitution at R′ is preferred for higher activities. The CoMSIA analysis show that hydrophobic effect is the only filed for the best CoMSIA model. The location of the white contours indicate that hydrophilic groups at R and R″ is likely to increase the activity. The docking analysis reveal that hydrogen bonding and CH···π interaction come into play in this type of molecules for docking with the COX-2 protein (1CX2). Molecular dynamics study nicely correlates with results obtained from the docking study. Current studies indicate that, in the design of better COX inhibitors, the aim should be to increase the polarities of three hydrogen bonding sites present on the molecules.

CONFLICT OF INTEREST

The authors declare that there is no conflict of interests regarding the publication of this article.

REFERENCES

1. S.D. Silberstein and J.C. Stirpe, *Expert Opin. Pharmacother.*, **15**, 1863 (2014); https://doi.org/10.1517/14656566.2014.937704.
2. D. Picot, P.J. Loll and R.M. Garavito, *Nature*, **367**, 243 (1994); https://doi.org/10.1038/367243a0.
3. R.G. Kurumbail, A.M. Stevens, J.K. Gierse, J.J. McDonald, R.A. Stegeman, J.Y. Pak, D. Gildehaus, J.M. iyashiro, T.D. Penning, K. Seibert, P.C. Isakson and W.C. Stallings, *Nature*, **384**, 644 (1996); https://doi.org/10.1038/384644a0.
4. A.S. Kalgutkar, B.C. Crws, S.W. Rowlinson, C. Garner, K. Seibert and L.J. Marnett, *Science*, **280**, 1268 (1998); https://doi.org/10.1126/science.280.5367.1268.
5. M. Laube, C. Tondera, S.K. Sharma, N. Bechmann, F.-J. Pietzsch, A. Pigorsch, M. Köckerling, F. Wuest, J. Pietzsch and T. Kniess, *RSC Adv.*, **4**, 38726 (2014); https://doi.org/10.1039/C4RA05650G.
6. A. Bhardwaj, J. Kaur, J. Wuest and E.E. Knaus, *ChemMedChem*, **9**, 109 (2014); https://doi.org/10.1002/cmdc.201300355.
7. P. Thirumurugan, S. Mahalaxmi and P.T. Perumal, *J. Chem. Sci.*, **122**, 819 (2010); https://doi.org/10.1007/s12039-010-0070-3.
8. A.V. Reddy, S. Gogireddy, P.K. Dubey, B.M. Reddy and B. Veeresh, *J. Chem. Sci.*, **127**, 433 (2015); https://doi.org/10.1007/s12039-015-0792-3.
9. C. Battilocchio, G. Poce, S. Alfonso, G.C. Porretta, S. Consalvi, L. Sautebin, S. Pace, A. Rossi, C. Ghelardini, L. Di Cesare Mannelli, S. Schenone, A. Giordani, L. Di Francesco, P. Patrignani and M. Biava, *Bioorg. Med. Chem.*, **21**, 3695 (2013); https://doi.org/10.1016/j.bmc.2013.04.031.
10. F. Wuest, X. Tang, T. Kniess, J. Pietzsch and M.X. Suresh, *Bioorg. Med. Chem.*, **17**, 1146 (2009); https://doi.org/10.1016/j.bmc.2008.12.032.

11. J. Grover, N. Bhatt, V. Kumar, N.K. Patel, B.J. Gondaliya, M. Elizabeth Sobhia, K.K. Bhutani and S.M. Jachak, *RSC Adv.*, **5**, 45535 (2015); https://doi.org/10.1039/C5RA01428J.
12. S. Consalvi, G. Poce, R. Ragno, M. Sabatino, C. La Motta, S. Sartini, V. Calderone, A. Martelli, C. Ghelardini, L. Di Cesare Mannelli and M. Biava, *ChemMedChem*, **11**, 1804 (2016); https://doi.org/10.1002/cmdc.201600086.
13. X. Lu, Z. Wang, S. Ren, F. Shen, R. Man and H. Zhu, *Bioorg. Med. Chem. Lett.*, **26**, 3491 (2016); https://doi.org/10.1016/j.bmcl.2016.06.037.
14. R. Fioravanti, A. Bolasco, F. Manna, F. Rossi, F. Orallo, F. Ortuso, S. Alcaro and R. Cirilli, *Eur. J. Med. Chem.*, **45**, 6135 (2010); https://doi.org/10.1016/j.ejmech.2010.10.005.
15. R. Ghodsi, E. Azizi and A. Zarghi, *Iran. J. Pharm. Res.*, **15**, 169 (2016).
16. S. Hasabelnaby, E.M. Mohi El-Deen and A. Goudah, *Antiinflamm. Antiallergy Agents Med. Chem.*, **14**, 148 (2015); https://doi.org/10.2174/1871523014666151103113544.
17. F.A. Ragab, H.I. Heiba, M.G. El-Gazzar, S.M. Abou-Seri, W.A. El-Sabbagh and R.M. El-Hazek, *MedChemComm*, **7**, 2309 (2016); https://doi.org/10.1039/C6MD00367B.
18. T. Shanmuganathan, K. Parthasarathy, M. Venugopal, Y. Arun, N. Dhatchanamoorthy and A.A.M. Prince, *J. Chem. Sci.*, **129**, 117 (2017); https://doi.org/10.1007/s12039-016-1209-7.
19. T.T. Dao, Y.S. Chi, J. Kim, H.P. Kim, S. Kim and H. Park, *Bioorg. Med. Chem. Lett.*, **14**, 1165 (2004); https://doi.org/10.1016/j.bmcl.2003.12.087.
20. A. Sarkar and G. Mostafa, *J. Mol. Model.*, **15**, 1221 (2009); https://doi.org/10.1007/s00894-009-0481-6.
21. R.D. Cramer, D.E. Patterson and J.D. Bunce, *J. Am. Chem. Soc.*, **110**, 5959 (1988); https://doi.org/10.1021/ja00226a005.
22. H. Kubinyi, G. Folkers and Y.C. Martin, 3D QSAR in Drug Design Kluwer: Dordrecht (1988).
23. G. Klebe, U. Abraham and T. Mietzner, *J. Med. Chem.*, **37**, 4130 (1994); https://doi.org/10.1021/jm00050a010.
24. A. Ali, D. Bansal, N.K. Kaushik, N. Kaushik, E.H. Choi and R. Gupta, *J. Chem. Sci.*, **126**, 1091 (2014); https://doi.org/10.1007/s12039-014-0671-3.
25. R. Bathini, S.K. Sivan, S. Fatima and V. Manga, *J. Chem. Sci.*, **128**, 1163 (2016); https://doi.org/10.1007/s12039-016-1103-3.
26. A. Misra, S. Sharma, D. Sharma, S. Dubey, A. Mishra, D. Kishore and J. Dwivedi, *J. Chem. Sci.*, **130**, 31 (2018); https://doi.org/10.1007/s12039-018-1430-7.
27. SYBYL-X 2.0, Tripos Inc, St. Louis.
28. S. Kaur and H.K. Kashyap, *J. Chem. Sci.*, **129**, 103 (2017); https://doi.org/10.1007/s12039-016-1207-9.
29. S. Indra and S. Daschakraborty, *J. Chem. Sci.*, **130**, 3 (2018); https://doi.org/10.1007/s12039-017-1404-1.
30. Y. Tamura, Y. Yoshimoto, K. Kunimoto, S. Tada, S. Matsumura, M. Murayama, Y. Shibata and H. Enomoto, *J. Med. Chem.*, **24**, 43 (1981); https://doi.org/10.1021/jm00133a010.
31. AbdulHameed, A. Hamza, J. Liu and C.-G. Zhan, *J. Chem. Inf. Model.*, **48**, 1760 (2008); https://doi.org/10.1021/ci800147v.
32. D.M. Hawkins, S.C. Basak and D. Mills, *J. Chem. Inf. Comput. Sci.*, **43**, 579 (2003); https://doi.org/10.1021/ci025626i.
33. P.P. Roy and K. Roy, *QSAR Comb. Sci.*, **27**, 302 (2008); https://doi.org/10.1002/qsar.200710043.